Proceedings of ASME Turbo Expo 2011
GT2011
June 6-10, 2011, Vancouver, British Columbia, Canada

GT2011-45936

COMPREHENSIVE APPLICATION OF A FIRST PRINCIPLES BASED METHODOLOGY FOR DESIGN OF AXIAL COMPRESSOR CONFIGURATIONS

Vishwas Iyengar, Ph.D.
Southwest Research Institute®
San Antonio, TX
Email: vishwas.iyengar@swri.org

Lakshmi N. Sankar, Ph.D.
Georgia Institute of Technology
Atlanta, GA
Email: lsankar@ae.gatech.edu

ABSTRACT

Axial compressors are widely used in many aerodynamic applications. The design of an axial compressor configuration presents many challenges. It is necessary to retool the design methodologies to take advantage of the improved accuracy and physical fidelity of these advanced methods. Here, a first-principles based multi-objective technique for designing single stage compressors is described. The study accounts for stage aerodynamic characteristics and rotor-stator interactions. The proposed methodology provides a way to systematically screen through the plethora of design variables. This method has been applied to a rotor-stator stage similar to NASA Stage 35. By selecting the most influential design parameters and by optimizing the blade leading edge and trailing edge mean camber line angles, phenomena such as tip blockages, blade-to-blade shock structures and other loss mechanisms can be weakened or alleviated. It is found that these changes to the configuration can have a beneficial effect on total pressure ratio and stage adiabatic efficiency, thereby improving the performance of the axial compression system.

INTRODUCTION

The compressor is one of the most important components within a gas turbine engine. An inherently complex high-speed flow coupled with highly loaded blades can make the efficient operation of the compression system a daunting task. In order to run the compressor efficiently, structural instabilities, excessive deformation of the structure, and flow instabilities such as stall and surge must be avoided or dealt with effectively. The fundamental operations of a multistage axial compressor were known and presented to the French Academie des Sciences [1-2] as early as 1853. Since then the working of a compressor has been studied extensively, and compressors have evolved significantly. The complex mechanism associated with the compressors makes its design a challenging task. Traditionally, designers have used a combination of analytical tools, commercially available data, and expertise in making design decisions. This approach leads to an evolutionary approach for steering the design towards safe realizable conditions and configurations. Although increasing the number of stages leads to higher overall pressure rise, it also increases the weight and length of the overall compression system.

From an aerodynamic perspective, a more precise 3-D design of the compressor blade is very important as this ensures optimal blade loading. The aerodynamics of a compressor blade is also closely linked to its structural and aeroacoustic responses. An increased loading on the compressor blades can cause increased structural deformations to the blade, eventually leading to structural failure. An inefficient design of the blades can inherently lead to increased acoustic response from the blade, from rotor-stator interactions and shock patterns. As discussed by Lakshminarayana [3] early designs transonic and supersonic compressors were failures. Bad compressor designs lead to poor efficiency and low reliability. Initially it was believed that the low efficiencies were due to the shock patterns alone. But after successive design failures it was recognized that the losses were attributable to flow blockages that are caused by the shocks. Since then significant improvements have been made in blading design, shock optimization and hub-to-tip design. A brief summary of the some of the early designs is given by Hawthorne [4]. Clearly, the design of the compression system is a multifaceted problem.

In the late 1940s and early 1950s, axial compressor and turbine design substantially relied on empirical correlations of data. Howell [5] and Carter et al [6] performed mean line design of axial compressors that relied on cascade data for flow deviation. Cascade data also provided information on profiles and secondary losses. Modern blade design methods can be classified broadly into two approaches, inverse and direct approaches. In inverse design methods [7-9], desirable flow features on the blade, such as pressure distribution and/or pressure loading distribution are specified and the blade geometry is computed in such way that the specified flow features are produced. If done efficiently, this design method can be applied successfully. In the direct [10-14] approach the blade geometry is analyzed directly by a CFD analysis and/or experiments. In this method either the parameters that directly influence the blade section are modified or the (x, y, z) coordinates of the existing blade geometry is altered. The geometry is subsequently analyzed and the influence of design variables on its overall performance is assessed.

Both the inverse and direct design methods discussed earlier have their advantages and disadvantages. For example, the direct method can sometimes be trial-and-error, especially when the design parameters are selected in an ad-hoc manner. But it has its advantages over the inverse design method, which usually requires a number of inputs, some of which are not always known (e.g. 3-D pressure distribution) so as to produce the desired flow features. Hence, the direct method, which generally does not need such detailed knowledge of the flow, is usually preferred. Although the direct design methods used thus far are effective, they do not perform basic blade parameterization, wherein the blade sections are rebuilt based on blade camber line and other parameters which affect the blade section. In order to consistently rebuild a three-dimensional compressor blade, the blade camber lines, thickness distributions and the blade stack line need to be approximated as functions of several key parameters. Since these parameters directly influence the blade section, it is more useful to use these parameters as design variables rather than sweeping or leaning existing blade geometry.

This study aims to develop and demonstrate a systematic investigation to understand the impact of stage design on compressor performance- total pressure ratio and adiabatic efficiency. A methodology will be presented whereby the rotor and stator blades are designed based on a parametric description of the blade surface design variables and subsequently optimized using a multi-objective optimization technique. A preliminary application of the proposed methodology was successfully performed by Iyengar [15]. Here a brief overview of the methodology is presented. A set of state of the art analysis and design tools are next selected and described along with the multidisciplinary formulation for compressor design. Then the design methodology is studied further and applied in a more comprehensive manner where a multiobjective optimization is performed, results for which are presented.

TOOLS AND FORMULATION

Here the tools used for the design methodology are described briefly. The study is multifaceted, one that incorporates high fidelity computational fluid dynamics and design tools such as design of experiments and response surface methods. A low order coupling involving one dimensional flow analysis and design tools has previously been performed with certain success, but a need for higher order flow analysis coupled with design tools for optimization of compressor stage still exists.

Figure 1 shows a flowchart briefly describing the methodology.

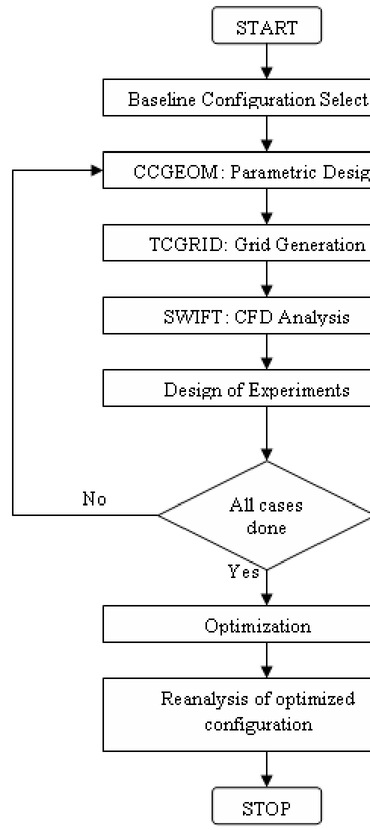

FIGURE 1: FLOWCHART SHOWING THE SEQUENCE OF EVENTS IN THE PROPOSED DESIGN METHODOLOGY.

In order to study compressor flow details, solution of the 3-D Navier-Stokes equations is necessary. Previously used analytical solutions are only valid to simple flows and configurations and therefore, numerical techniques are needed for more complex problems. In an effort to accurately model the flow within a compression system in this study, a very robust flow solver SWIFT, developed by Chima [16], is used.

The author refers to Chima [16] for details on the governing equations, boundary conditions and time marching approach used for this study. The k-ω SST turbulence model is used to model the effects of turbulent mixing in the compression system. The k-ω SST turbulence model is a high fidelity model and it most accurately captures the complex flow structure in an axial compressor configuration. For the grid generation, a three-dimensional grid code for turbomachinery-

TCGRID developed by Chima [17] at NASA Glenn Research Center is utilized in this study. This code is capable of generating single block grids as well as multi-block grids. The single block grids can be of either the H-type or C-type, whereas the multi-block grids must be a C-type grid around the blade.

This study uses a number of tools to complete the design process. A method to parametrically design the axial compressor blades is briefly described here; a more detailed discussion is included in Reference [18].

Parametric Blade Design

In an effort to parametrically model the compressor blades in this study, a tool originally developed by Wood [19] called CCGEOM, is used. The tool can be used to facilitate the rapid generation of the flow passage and blading for turbomachinery components. The tool uses a piece-wise smooth cubic spline interpolation method to obtain the geometry. First, the hub and tip geometries are supplied by the user as inputs by specifying the cylindrical co-ordinates (radial and axial) along each surface. In this study blade camber line angles and thicknesses at three chord-wise (leading edge, mid-chord and trailing edge) points and three different (hub, mid-span and tip) spanwise locations were specified for convenience. The present methodology is not restricted to specification of the blade geometry at these three locations. For more complex geometries, blade geometry may be specified at more locations.

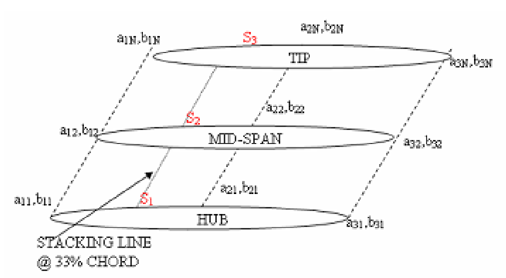

$a_{M,N}$ = *Blade mean camber line angle at chord location 'M' and span location 'N*

$b_{M,N}$ = *Blade thickness at chord location 'M' and span location 'N'*

S_N = *Blade section at span location 'N'*

FIGURE 2: SUMMARY OF PARAMETRIC BLADE DESIGN BASED ON DESIGN VARIABLES- $A_{M,N}$, $B_{M,N}$

Design of Experiments

When designing the blades, a number of design variables may be involved. The Design of Experiments technique used to sift through these design variables is discussed here briefly. The above parametric model gives rise to a number of parameters or “design variables” that may be generated to produce a family of blade surfaces. An independent change (say two possible changes) to each of these N values will give rise to 2^N combinations, a very large design space. Design of Experiments (DoE [18]) is a systematic way to plan, conduct and analyze a series of tests, where the input variables are changed systematically to extract intelligent information. This method uses a statistical approach that predicts the influences of variables along with their interactions on the responses, without the need for a full factorial analysis. By using DoE, the needed information can be extracted with less time and cost. Several methods have been developed to carry out the design of experiments, but the main purpose of each method is the same, which is to reduce the number of cases required to run whilst extracting more information from them.

Response Surface Methodology

An optimization method is needed to obtain the optimum settings for the design variables considered. Such a technique, called the Response Surface Method, is introduced here. For this work, the use of an all-encompassing model of the physical environment is required in order to explore the design space. The exploration of a complex design space requires the use of a Response Surface Methodology (RSM). In this study, a commercial software- JMP© [20] is used to perform the response surface optimization. RSM acts as a means to find the optimal settings of input factors or design variables that maximize, minimize or target measured responses or outcome variables. It utilizes Response Surface Equations (RSE’s) that take the form of a polynomial approximation of the relationships across given ranges for the input variables.

Output Variables Calculation

In a compression system the overall pressure ratio increases. The total pressure ratio is a measure of the increase in the pressure of the compression system. Total pressure ratio (TPR) of a compression system is defined as the ratio between the total pressure exiting the compressor to the total pressure entering the compressor. If the pressure exiting the compressor is P_{02} and the pressure entering the compressor is P_{01} then the TPR is defined as:

$$TPR = \frac{P_{02}}{P_{01}} \qquad \text{.. (1)}$$

The adiabatic efficiency of a compressor is the ratio of the ideal input work needed to raise the total pressure of a working fluid from a pressure value P_{01} to a new value P_{02}, to the actual work needed on the fluid. The adiabatic efficiency (η_{ad}) of the compression system can be found by using:

$$\eta_{ad} = \frac{W_S}{W_A} \qquad \text{.. (2)}$$

where W_S and W_A are the isentropic and actual work done on the flow, respectively. These can be found as follows:

$$W_S = \dot{m} c_p (\overline{T}_{02}|_s - \overline{T}_{01})$$

$$W_A = \dot{m} c_p (\overline{T}_{02} - \overline{T}_{01}) \quad .. (3)$$

where $\overline{\overline{T}}_{01}$ and $\overline{\overline{T}}_{02}$ are the total temperature are the original total temperature and the new total temperatures respectively. By applying isentropic relationship for points 1 and 2 as follows:

$$\frac{\overline{T}_{02}}{\overline{T}_{01}}\Big|_s = \left(\frac{\overline{p}_{02}}{\overline{p}_{01}}\right)^{\frac{\gamma-1}{\gamma}} \quad .. (4)$$

the bar quantities $\overline{\overline{p}}, \overline{\overline{T}}$ are obtained by the mixed-out averaging technique. By substituting equations (3) and (4) into equation (2), gives :

$$\eta_{ad} = \frac{\left(\frac{\overline{p}_{02}}{\overline{p}_{01}}\right)^{\frac{\gamma-1}{\gamma}} - 1}{\frac{\overline{T}_{02}}{\overline{T}_{01}} - 1} \quad .. (5)$$

In order to gain accurate noise prediction via CFD, it is important to ensure the boundary conditions used impose non-reflecting boundary conditions. The boundary conditions as used ensure that non-reflecting properties are imposed at the boundaries. The acoustic method adopted in this study computes the rotor-wake/stator interactions through coupled computation. Rotor wake profiles are established with three dimensional computations.

A Rotor Wake Influence Coefficient (RWIC) is defined to estimate the acoustic sound level generated by the rotor-wake/stator interactions at the rotor/stator exit.

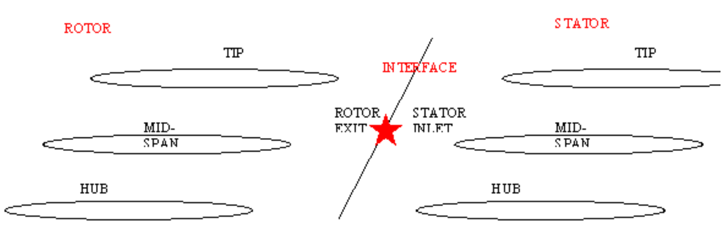

FIGURE 3: SCHEMATIC DIAGRAM SHOWING THE INTERFACE LOCATION USED FOR THE AEROACOUSTIC ANALYSIS.

Figure 3 shows the axial and circumferential location where the RWIC is calculated. Here RWIC is defined as:

$$RWIC = 10\log_{10}\left(P_{AMP} / P_{REF}\right) \quad .. (6)$$

where P_{REF} is the reference power equal to 20μPa and P_{AMP} is the root mean square fluctuating pressure amplitude at the rotor/stator interface defined as:

$$P'_{AMP} = \sqrt{\left(\frac{P_1'^2 + P_2'^2 + P_3'^2 + \cdots + P_n'^2}{n}\right)} \quad .. (7)$$

where $P_1', P_2' .... P_n'$ are the fluctuating pressures on each blade-to-blade mesh point at mid-span. The fluctuations are extracted from CFD results based on a circumferentially averaged pressure quantity at mid-span. Pressures at each blade-to-blade mesh point at mid span are subtracted from the circumferentially averaged pressure to give the fluctuating pressure profile. Upon obtaining the RWIC at each point, the RWIC value will be used in the optimization loop as an objective function. Benefits of using such method based on steady-state CFD solutions instead of using unsteady-state CFD solutions for the pressure levels calculation is that it is computationally less intensive, yet the RWIC value provides a way to measure the acoustic disturbance generated by the rotor wake onto the stator.

The sources contributing to compressor noise can originate at different locations in the compression system- on the blade, in the tip gap, rotor-stator interface etc. Typically noise generated due to rotor/stator interaction is considered to be important when carrying out a compressor stage design. Hence the use of RWIC at rotor-stator interface as an objective function is justified.

COMPREHENSIVE APPLICATION

Results from the comprehensive application of the design methodology are presented here. This method has been applied to a rotor-stator stage similar to NASA Stage 35. The newly optimized configuration is termed 'Optimized Configuration' for the entirety of the paper. Results are presented first in form of performance maps. The visualization of the flowfield is used to interpret the results. Results from the aeroacoustic analysis are also presented to substantiate the aerodynamic findings.

Selection of Design Variables

Eighteen variables were considered for screening; nine for the rotor and nine for the stator- camber line angles at three chord-wise (leading edge, mid-chord and trailing edge) points and three different (hub, mid-span and tip) spanwise locations. The objective functions, which in this case were total pressure ratio, adiabatic efficiency and rotor wake influence coefficient (RWIC), are obtained from CFD analysis performed in design of experiments. Pareto curves for total pressure ratio, adiabatic efficiency and RWIC are used to narrow the design variables based on their contributions. Only common variables that account for approximately 90% contributions to the total pressure ratio, adiabatic efficiency, and RWIC, are selected.

A closer look at the variables shows, as expected, that the prominent variables are primarily associated with the rotor blade, as compared to the stator blade. This evidently means that, when compared to the stator, the design of the rotor has a greater impact on the compressor stage performance functions considered in this study.

In a previous study, equal numbers of rotor and stator design variables were chosen as design variables. Although it led to a preliminary configuration, the screening performed in this section suggests that a larger set of variables is necessary, especially from the rotor design. Ten variables were selected based on its variability (common variables that account for approximately 90% contributions to objective functions), are selected as the decisive design variables for the design of the compressor stage. The variables are split such that 8 variables are for the rotor and the other 2 are for the stator. The design of experiments is performed again for the 10 variables. Subsequently a multi-objective optimization was performed with the 10 selected variables where the total pressure ratio, adiabatic efficiency and RWIC were equally weighted. The optimizer was executed with the intent of maximizing the stage adiabatic efficiency, stage total pressure ratio and minimizing the rotor wake influence coefficient across the rotor-stator interface.

Optimization Results

Performance map comparisons

Performance maps for the starting configuration and the optimized configuration are shown on Figure 4 where the total pressure ratio of the stage is plotted as function of the ratio of the mass flow rate to the choking mass flow rate of the respective configurations.

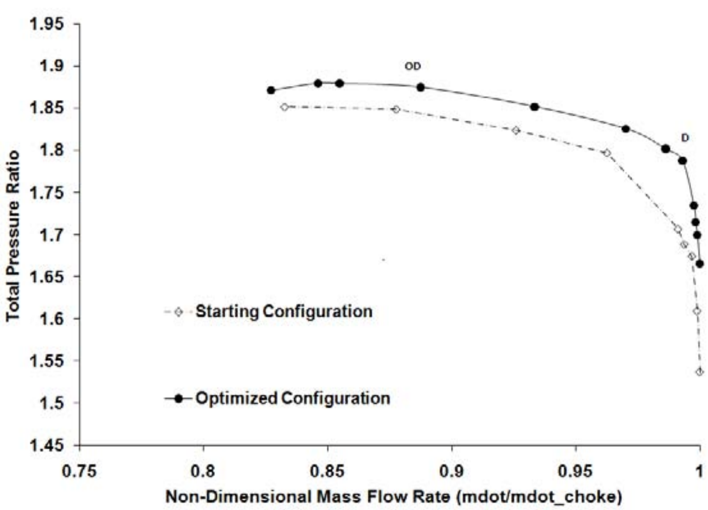

FIGURE 4: PERFORMANCE MAP COMPARING THE STARTING CONFIGURATION TO THE OPTIMIZED CONFIGURATION.

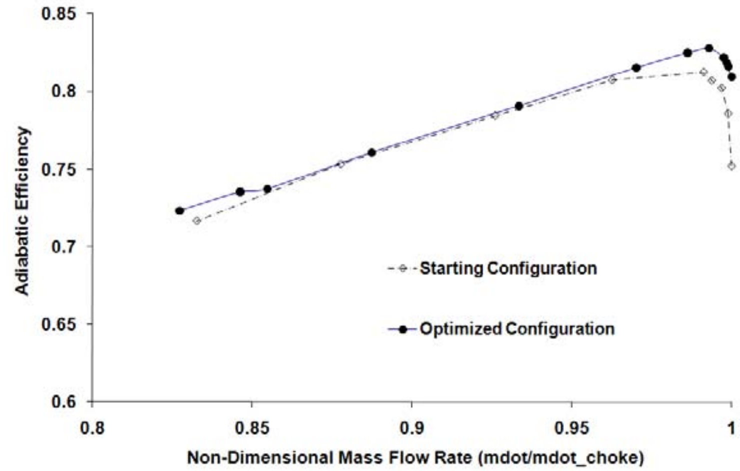

FIGURE 5: ADIABATIC EFFICIENCY MAP COMPARING THE STARTING CONFIGURATION TO THE OPTIMIZED CONFIGURATION.

For the optimized configuration, the choking point was found to be 20.76 kg/sec, compared to 19.8 kg/sec for the starting configuration. On comparing the optimized configuration to the starting configuration, it can be noticed that the optimized case exhibits on average a 2.5% increase in total pressure ratio over the entire operating range. The operating range for the optimized configuration shows a slight improvement over the starting configuration. Figure 5 shows the adiabatic efficiency map for the two configurations. From the efficiency map it can be observed that the difference in peak adiabatic efficiency between the two configurations is significant, especially at peak-efficiency. Near choke conditions, the optimized configuration has 2.5% higher peak efficiency than the starting configuration, which is quite substantial. Some adiabatic efficiency benefits for the optimized configuration are also seen at lower mass flow rates.

Assessment of Blade Loading

In order to make an assessment of the blade performance, the change in blade loading is considered. Figure 6 (rotor) and Figure 7 (stator) show the blade loading comparison between the starting and optimized configurations at three spanwise locations (hub, mid span and tip). In the figures the non-dimensional static pressures are plotted against position on the blade. Usually the area under such a loading curve is a measure of the amount of loading on the blade surface. It can be said that the higher the area under the curve, the greater the loading on the blade. The increased loading corresponds to the blade doing more work on the flow, which can result in higher stage total pressure ratio.

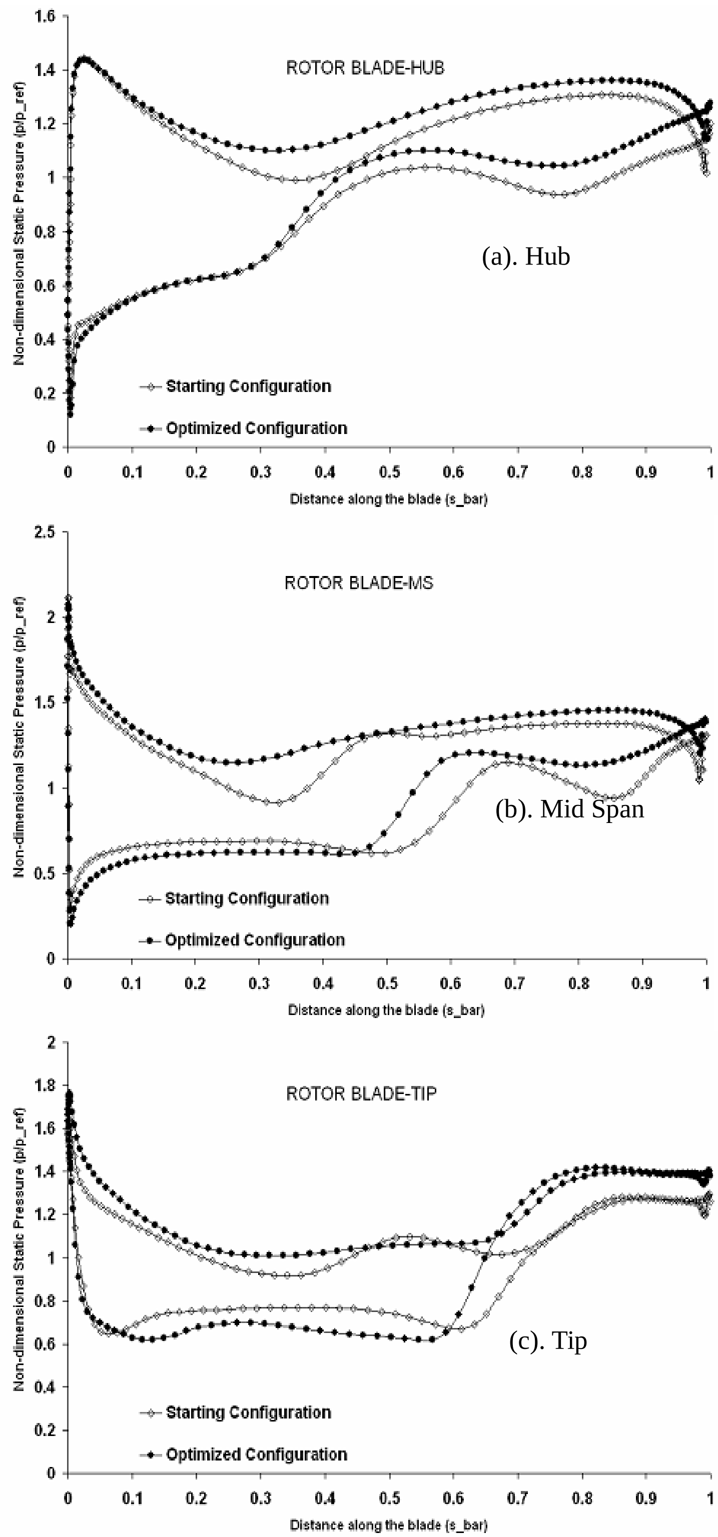

FIGURE 6: ROTOR BLADE LOADING CURVE COMPARISON AT (A) HUB, (B) MID SPAN AND (C) TIP BETWEEN THE STARTING CONFIGURATION AND OPTIMIZED CONFIGURATION.

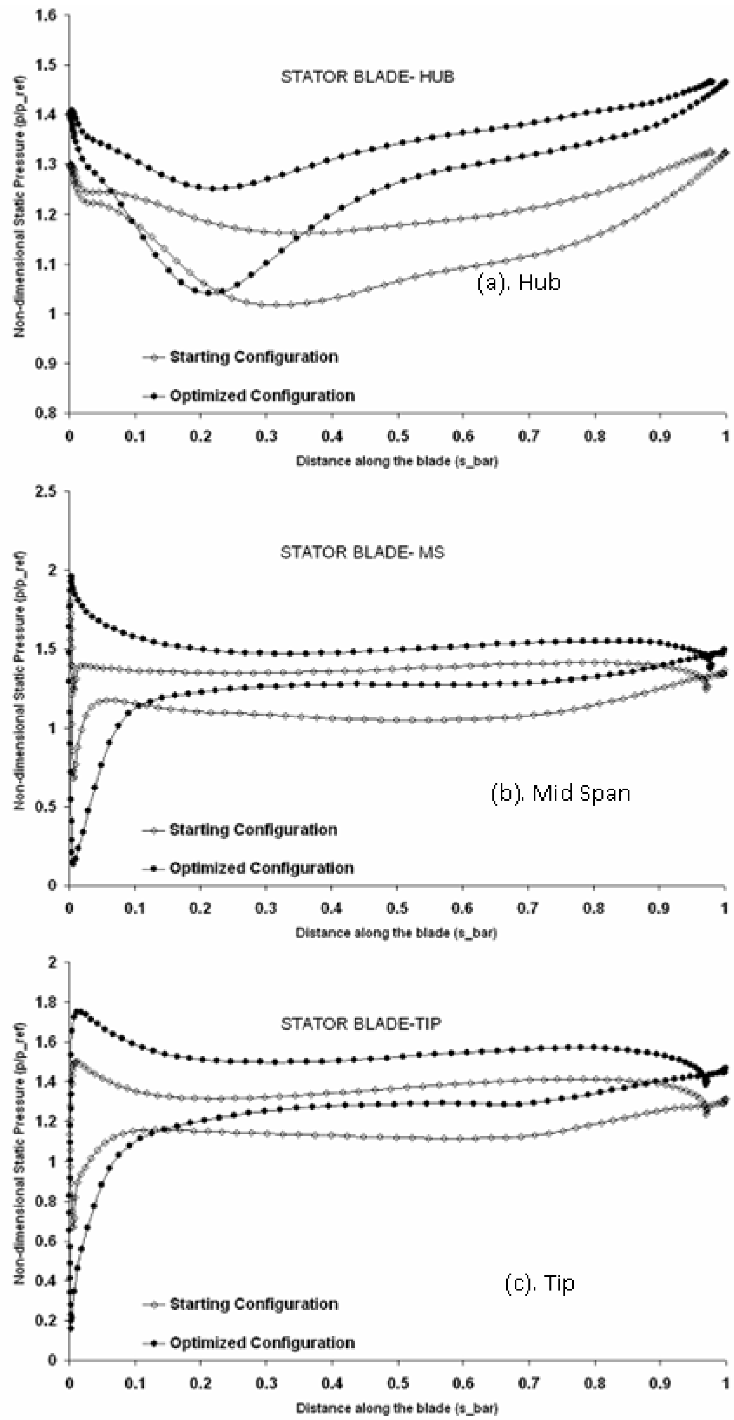

FIGURE 7: STATOR BLADE LOADING CURVE COMPARISON AT (A) HUB, (B) MID SPAN AND (C) TIP BETWEEN THE STARTING CONFIGURATION AND OPTIMIZED CONFIGURATION.

From Figure 6 it is noticed that the optimized rotor blade experiences a slight increase in blade loading at the hub (Figure 6a), mid span (Figure 6b) and tip (Figure 6c) when compared to the starting configuration rotor blade, especially at the rotor leading edge. For the stator blade it is clear that the optimized configuration has an increased blade loading at mid span (Figure 7b) and tip (Figure 7c) when compared to the starting configuration. The blade incidence has also been significantly changed going from the starting configuration to the optimized configuration. The change in incidence can better align the blade to the flow and also alter the direction of the tip vortex. A detailed discussion on direction of tip vortex and its effects on blockages and stage performance will be presented later.

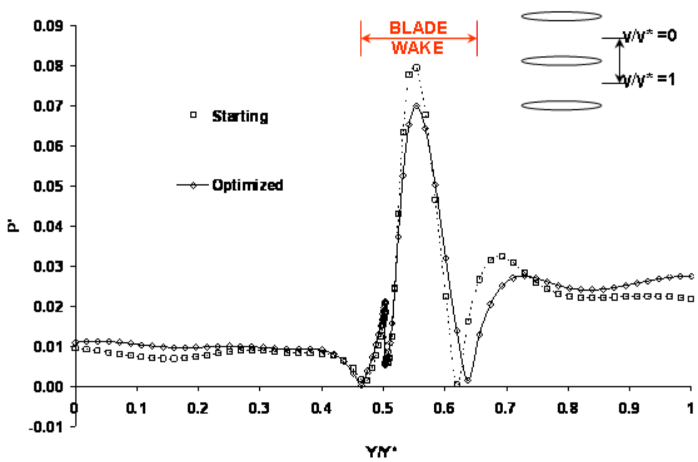

FIGURE 8: COMPARISONS OF THE BLADE-TO-BLADE PRESSURE FLUCTUATION INFLUENCING THE ROTOR-WAKE/STATOR INTERACTIONS AFT OF THE ROTOR BLADE AT MID-SPAN.

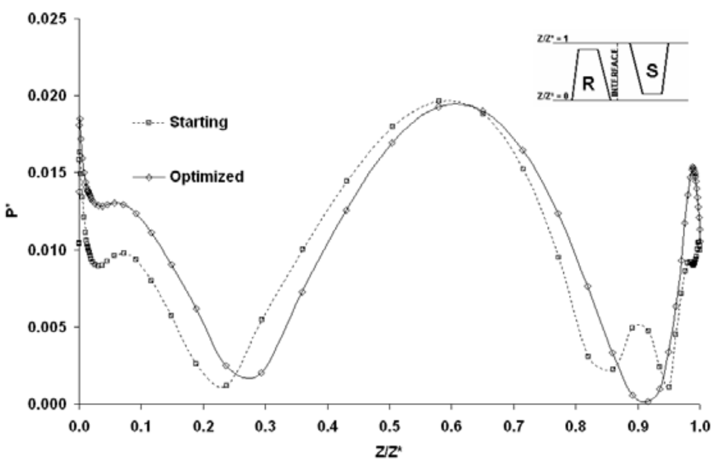

FIGURE 9: COMPARISONS OF THE HUB-TO-TIP PRESSURE FLUCTUATIONS INFLUENCING THE ROTOR-WAKE/STATOR INTERACTIONS AT ROTOR-STATOR INTERFACE.

Rotor-Stator aeroacoustic interaction comparisons

In order to evaluate the rotor-stator interactions, the blade-to-blade pressure fluctuations at mid-span and mid passage are monitored in the CFD analysis. The pressure fluctuations caused by the rotor design provide a way to quantify the potential disturbances and noise that may propagate downstream.

Figure 8 shows a plot comparing the blade-to-blade pressure fluctuations at rotor exit (stator entrance) for both the starting and optimized configurations. The fluctuations are measured about a circumferentially averaged pressure value at mid-passage. In the plot the y-axis shows the fluctuating pressures (P') and the x-axis represents the blade-to-blade circumferential location where y/y* = 0 and y/y* = 1 are labeled. It can be observed from the figure that the pressure fluctuations aft of the rotor blade are less for the optimized configuration compared to the starting configuration at most of the circumferential location. Also the magnitude of the pressure fluctuations in the blade wake region is smaller for the optimized configuration when compared to the starting configuration. In the region y/y*=0.6 to y/y* = 1.0, it can be observed that the optimized configuration has smaller magnitude and smaller fluctuations when compared to starting configuration.

Figure 9 shows the pressure fluctuations in the radial direction, from the hub to the tip. Here the fluctuations are measured about a radially averaged pressure value. In the plot the y-axis shows the fluctuating pressures (P') and the x-axis represents the hub-to-tip radial location where z/z* = 0 and z/z* = 1 are labeled. In the region z/z* = 0.25 to z/z* = 0.9, it is observed that the optimized configuration has slightly smaller magnitude and smaller fluctuations when compared to starting configuration. In the tip section (z/z* = 0.975) the optimized configuration has slightly higher P' magnitude when compared to the starting configuration.

Flowfield comparisons

The flow fields for the starting and optimized configurations are compared to quantify the differences observed in the performance maps. Flowfield comparisons are performed for off-design condition (87% choke massflow) 'OD' and the design point 'D' (97% choke massflow) as shown on performance map in Figure 6. In Figure 10, the directions of the rotor leading edge tip vortex for the starting configuration and the optimized configuration are compared. The strengths of the tip vortex are also compared by superimposing the entropy on the particle path. Two notable differences can be observed. Firstly, the direction and width of the tip vortex for the optimized configuration has been significantly altered as it is seen that the tip vortex moves away from the neighboring blade and is narrower. Secondly, it is observed that the tip vortex entropy strengths are weaker for the optimized configuration when compared to the starting configuration. The reduced entropy strength along with the altered tip vortex direction results in reduced blockages in the mid-passage section and will have significant aerodynamic performance benefits. The altered tip vortex direction can be correlated to the changed rotor blade incidences.

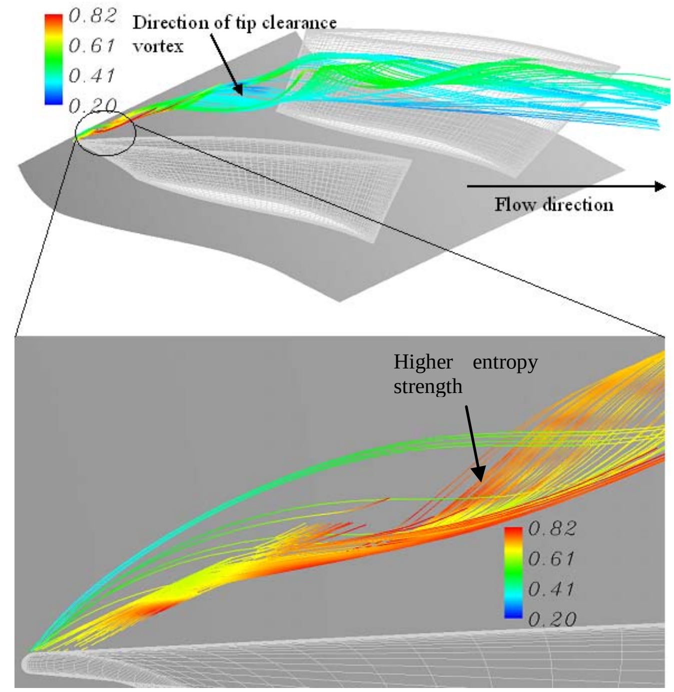

(a). Starting Configuration

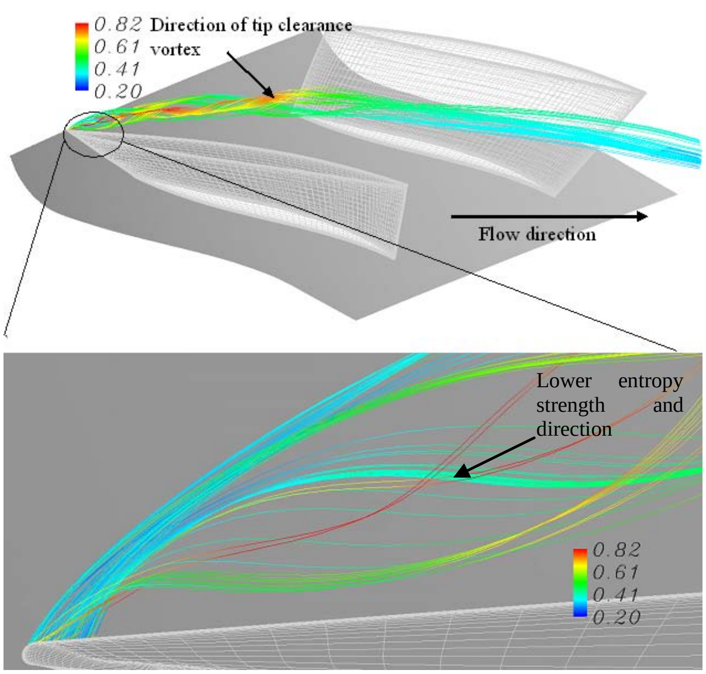

(b). Optimized Configuration

FIGURE 10: DIRECTION AND ENTROPY STRENGTH OF THE ROTOR LEADING EDGE TIP VORTEX.

Figure 11 compares the entropy contours at mid-passage in the meridional plane for the starting and optimized configurations at the off-design condition. For the starting configuration a significant region of high entropy exists in the tip section near the leading edge. This high entropy is attributed to the tip clearance vortex discussed previously. It is noticed that the casing boundary layer is separated near the rotor leading edge because of the shock and the clearance vortex interactions. In case of the optimized configuration a less pronounced region of high entropy is observed at the rotor tip, suggesting that the strength of shock-clearance vortex interaction is lesser for the optimized configuration. Similar result was also observed in Figure 10.

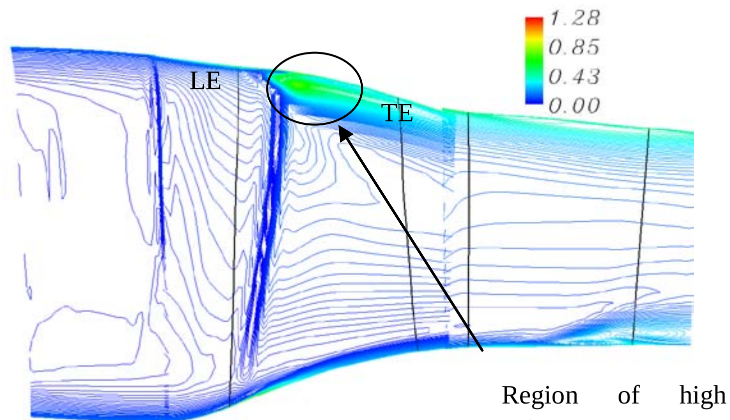

(a). Starting Configuration

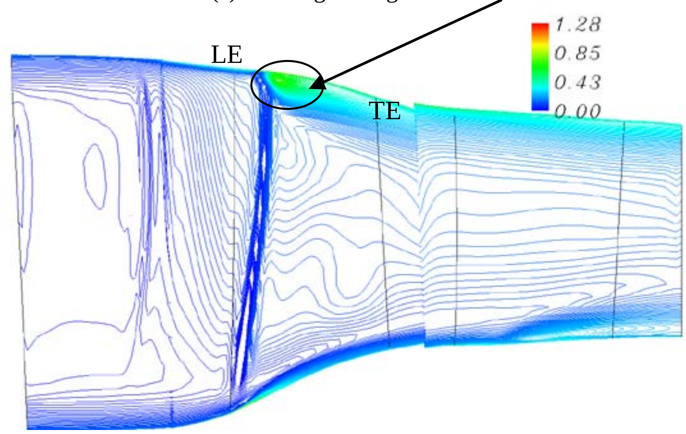

(b). Optimized Configuration

FIGURE 11: ENTROPY (NON-DIMENSIONAL) CONTOUR COMPARISON BETWEEN THE (A). STARTING AND (B). OPTIMIZED CONFIGURATIONS, FOR MID PASSAGE LOCATION AT OFF-DESIGN CONDITION.

Figure 12 compares the entropy contours for an off-design condition for the starting configurations and optimized at tip clearance section in the blade-to-blade plane. Here the single passage results have been periodically rotated to reflect adjacent blade passages. On Figure 12a, three areas are marked as A- ahead of the blade, B- near the rotor leading edge above the blade and C- mid passage wake region. At point A, the region of high entropy previously present for the starting configuration is now non-existent for the optimized case. At the leading edge (Point B) a very rapid change of entropy is noticed, this is caused by the shock which is relatively weaker for the optimized case compared to the starting. In the mid passage wake region (Point C), the blade-to-blade wake entropy strength for the optimized configuration is significantly lower than that for the starting configuration.

Overall, this indicates that the blockages both upstream and downstream of the rotor blade are reduced. This has a substantial influence on the performance of the rotor especially at off-design conditions such as the one shown. The improvement in the wake region also effects the rotor wake-stator noise interactions and substantiates the reduced levels of aero-acoustic interactions found earlier for the optimized configuration.

Mach number contours comparing the starting and optimized configuration at 90% span location from the hub for off-design condition is shown on Figure 13. On Figure 13a smeared shock emerging from the pressure side (labeled A) at the rotor leading edge can observed for the starting configuration. This shock passes through the entire passage eventually ending at the suction side of the next blade. In the process the shock interacts with the boundary layer on the upper surface of the next blade and can at times trigger boundary layer separation. From Figure 13b it is noticed that the shock emanating from the rotor pressure side does not exist for the optimized configuration. Instead a weaker detached shock that loses its strength before it can reach the neighboring rotor blade is observed, and the detached shock does not affect the flow on the suction side of the next rotor blade.

Figure 14 shows the effects of the shock and clearance flow on the casing boundary layer. Blade-to-blade plot of Mach number contours for starting (Figure 14a) and optimized configuration (Figure 14b) at the blade tip- off design condition are shown at the right of the figure. This close to the casing the shock is highly smeared, and the tip vortex can be followed through the shock to the pressure side of the neighboring blade. Two meridional plots of Mach number contours above 70 percent span at two tangential locations (20% and 40%) are shown on the left. The leading edge and trailing edges are also shown for reference.

In Figure 14a, the bottom left plot is near the suction surface of the blade shows the clearance vortex just downstream of the leading edge, followed by a region of low-speed flow. The shock is evident at near 50% chord, followed by an even larger region of low-speed flow caused by the shock-boundary layer interaction. At 40% tangential location the clearance vortex is evident at approximately 30% chord. The dotted arrow shows the propagation of the vortex in the azimuthal direction. The solid arrow indicates the chordwise distance of the clearance vortex from the leading edge.

For the optimized configuration, it is observed from Figure 14b that the azimuthal convection of the clearance vortex is slightly different. The tip vortex for the optimized configuration appears to be traveling at higher angle relative to the normal when compared to Figure 14b. Also the chordwise position of the same clearance vortex is at a greater chordwise location (~45%), which is again indicated by the longer solid arrow with leading edge as the reference. By altering the propagation direction of the tip clearance vortex for the optimized configuration, any blockage effects due to the interaction between the tip vortex and blade-to-blade shocks are reduced.

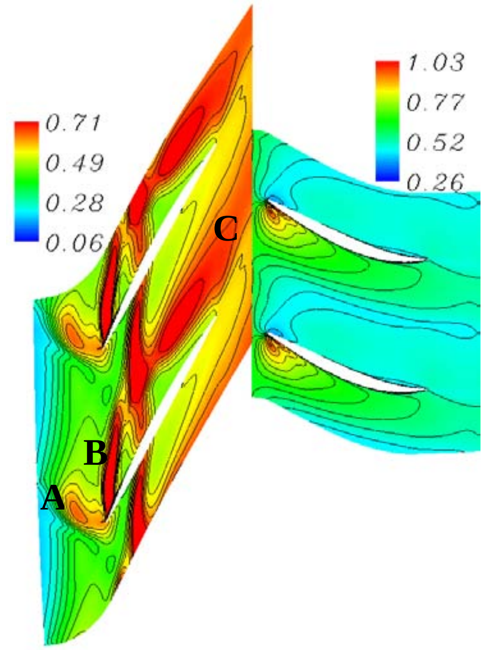

(a). Starting Configuration

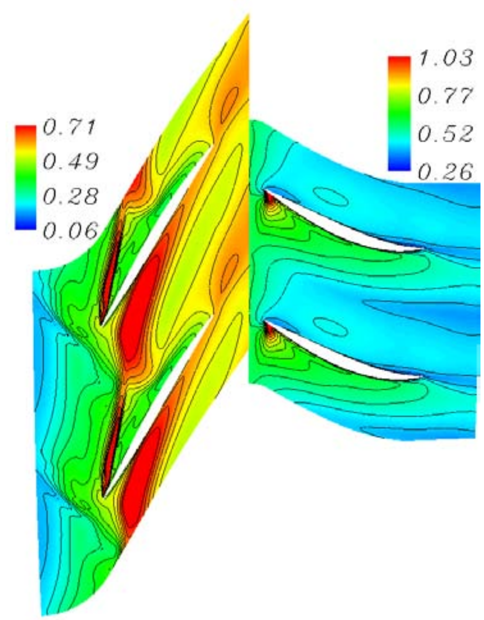

(b). Optimized Configuration

FIGURE 12: ENTROPY (NON-DIMENSIONAL) CONTOUR COMPARISON BETWEEN THE (A). STARTING AND (B). OPTIMIZED CONFIGURATIONS, FOR TIP CLEARANCE SECTION AT OFF-DESIGN CONDITION.

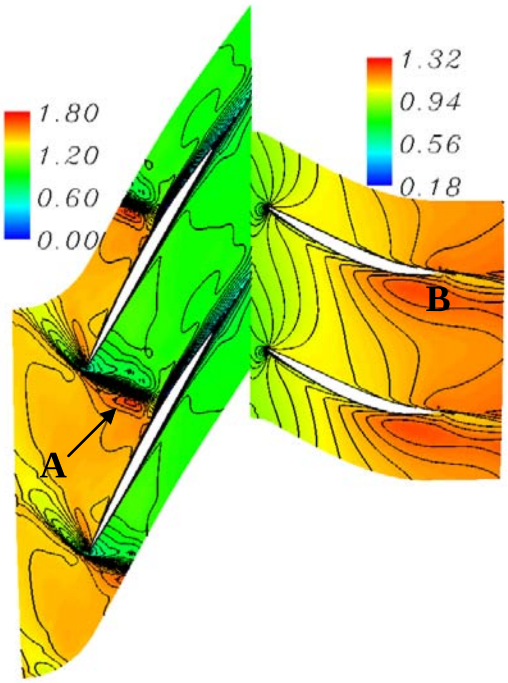

(a). Starting Configuration

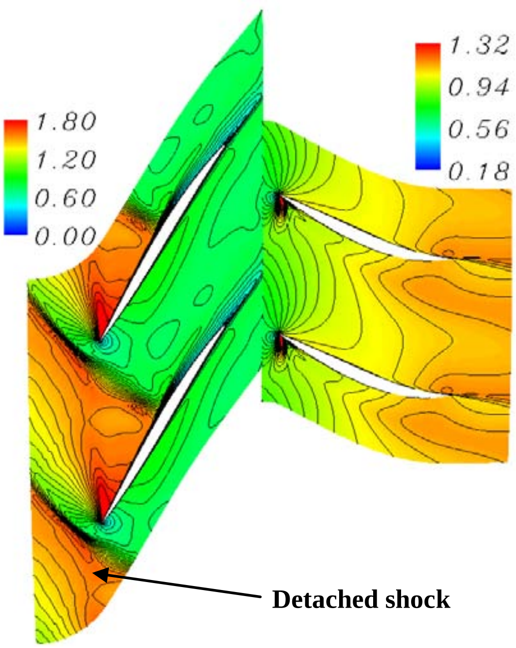

(b). Optimized Configuration

FIGURE 13: MACH NUMBER CONTOUR COMPARISON BETWEEN THE (A). STARTING AND (B). OPTIMIZED CONFIGURATIONS AT 90% SPAN FROM HUB AT OFF-DESIGN CONDITION.

In the blade-to-blade plane on the right side of Figure 14a, a strong shock emerging from the suction side of blade leading edge is evident for the starting configuration. Comparing this shock to its counterpart in the optimized configuration in Figure 14b, it is seen that this shock for the latter is not as strong as the one for the starting configuration. The shock for the optimized configuration is also not as smeared as compared to the starting configuration and does not extend through the entire passage. It is noticed again that the interactions between the shock emerging from pressure side and the neighboring blade are very minimal for the optimized configuration compared to the starting one.

Here it is found the aerodynamic changes have a beneficial effect on the performance of the compressor stage. It can be construed that the blockage modifications and reduced shock strengths result in increased total pressure ratios across the stage for no additional penalty in the form of decrease in adiabatic efficiency.

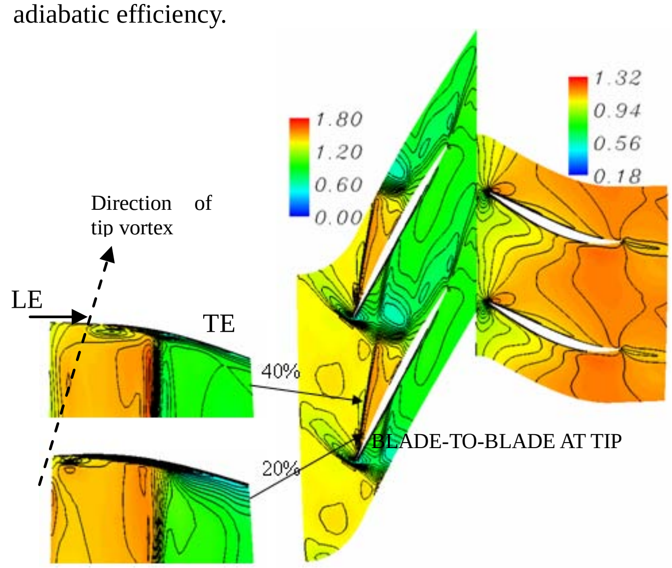

(a). Starting Configuration

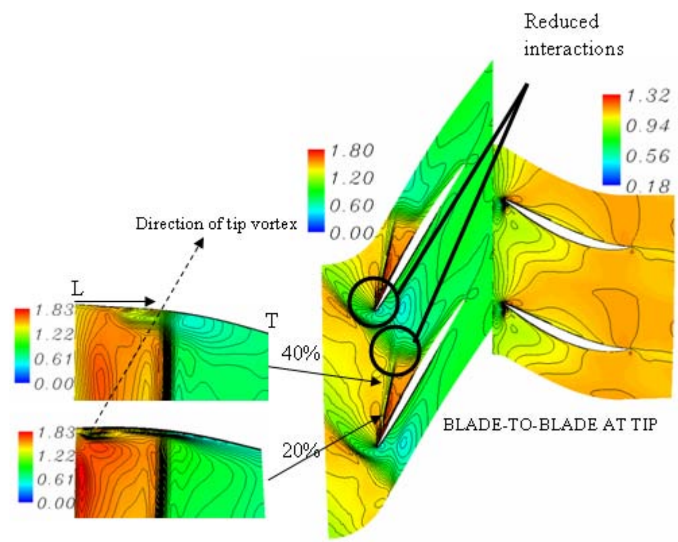

(b). Optimized Configuration

FIGURE 14: MACH NUMBER CONTOUR COMPARISON BETWEEN THE (A). STARTING AND (B). OPTIMIZED CONFIGURATIONS AT TIP OFF-DESIGN CONDITION AND TWO MERIDIONAL PLANES ABOVE 70% SPAN.

CONCLUSIONS

A first-principles based method to design axial compressor blade configurations has been developed. A systematic study of the effects of blade design parameters on compressor performance has been done. As a part of the work several aspects of blade design- aerodynamics and aeroacoustics behavior have been studied. A combination of performance map data and flow visualization studies have been used to report the findings.

Based on these studies, the following conclusions can be drawn:

- The parametric design of an axial compressor configuration requires a number of advanced tools. The fidelity level of these tools dictates the accuracy and effectiveness of the design process. The operation of modern compressor processes is very complex and affected by nonlinear effects such as shocks, tip vortices, and blockages. High fidelity tools are therefore necessary. Such high fidelity tools have been extensively explored in this study.
- In designing an axial compressor stage a large number of design variables are involved. These include design variables associated with the rotor and the stator blades, resulting in a large set of design of experiments. It was found that the variables associated with the rotor have a bigger influence on the response(s) compared to the stator blade variables.
- Axial compressor blades are very sensitive to alterations in blade topology. It was found that by optimizing the blade leading edge and trailing edge mean camber line angles, phenomena such as tip blockages, blade-to-blade shock structures and other loss mechanisms can be weakened or alleviated. These can have a beneficial effect on total pressure ratio and stage adiabatic efficiency, therefore improving the performance of the axial compression system.
- It was found that an aerodynamically optimized blade can also have aeroacoustic benefits. By optimizing the blade trailing edge, the fluctuating aeroacoustic signature from rotor to stator is minimized, therefore resulting in lower rotor wake-stator interactions.

ACKNOWLEDGMENTS

This work was carried out under a program sponsored by National Aeronautics and Space Administration (NASA) and the Department of Defense. The authors would like to thank Dr. Rodrick V. Chima at NASA Glenn Research Center for his assistance in this study.

REFERENCE

[1] Horlock, J. H., Axial Flow Compressors, Butterworths Scientific Publications, London, 1958.
[2] Gostelow, J. P., Cascade Aerodynamics, Pergamon Press, New York, NY, 1984.
[3] Lakshminarayana, B., Fluid Dynamics and Heat Transfer of Turbomachinery, John Wiley and Sons. Inc, 1996.
[4] Hawthorne, W.R., Aerodynamics of Turbines and Compressors, Princeton University Press, Princeton, NJ, 1964.
[5] Howell, A. R., "The Present Basis of Axial Flow Compressor Design: Part 1- Cascade Theory and Performance," Aeronautical Research Council R. and M. No. 2095, 1942.
[6] Carter, A. D. S., and Hughes, H. P., "A Theoretical Investigation of the Effect of Profile Shape on the Performance of Aerofoil's in Cascade," Aeronautical Research Council R. and M. No. 2384, 1950.
[7] Stanitz, J. D., "Design of Two-Dimensional Channels with Prescribed Velocity Distributions along the Channel Walls," NASA Tech. Notes 2593-2595, 1952.
[8] Katsanis, T., "A Computer Program for Calculating Velocities and Streamlines for Two-Dimensional, Incompressible Flow in Axial Blade Rows," NACA Technical Note, NASA TN D- 3762, January 1967.
[9] Hu, P., and Zangeneh, M., "On Design of Transonic Fan Rotors by 3D Inverse Design Method," Proceedings of GT2006, ASME Turbo Expo 2006, GT2006-91173.
[10] Bolger, J. J., and Horlock, J. H., "Predictions of the Flow in Repeating Stages of Axial Compressors Using Navier-Stokes Solvers," ASME Paper 95-GT-199, 1995.
[11] Hah, C., and Wennerstrom, A. J., "Three-Dimensional Flowfields Inside a Transonic Compressor with Swept Blades," Journal of Turbomachinery, Vol. 113, pp. 241-251, 1991.
[12] Wadia, A. R., Szucs, P. N. and Crall, D. W., "Inner Workings of Aerodynamic Sweep," ASME Journal of Turbomachinery, Vol. 120- No. 4, pp. 671-682, 1998.
[13] Denton, J.D., amd Xu, L., "The Effects of Lean and Sweep on Transonic Fan Performance," ASME Paper GT-2002-30327, 2002.
[14] Keshin, A., Dutta, A. K., and Bestle, D., "Modern Compressor Aerodynamic Blading Process Using Multi-Objective Optimization," Proceedings of GT2006, ASME Turbo Expo 2006, GT2006-90206.
[15] Iyengar, V., Sankar L.N., and Denney R., "A First-Principle Based Methodology for Design of Axial Compressor Configurations," Proceedings of GT2007, ASME Turbo Expo 2007, Montreal, GT2007-27513.
[16] Chima, R. V., "Swift - Multiblock Analysis Code for Turbomachinery, User's Manual and Documentation," Version 300, Sept. 2003.
[17] Chima, R. V., "TCGRID 3-D Grid Generator for Turbomachinery, User's Manual and Documentation," Version 300, July, 2003.
[18] Iyengar., V "A First-Principle Based Methodology for Design of Axial Compressor Configurations," Ph.D. Thesis, School Of Aerospace Engineering, Georgia Institute of Technology August 2007.
[19] Wood, J. R., "CCGEOM User Manual," Feb. 1997.
[20] JMP, A Business Unit of SAS "Using JMP- USER MANUAL," October 2010.

